Orbital electron densities of ethane: Comparison of electron momentum spectroscopy measurements with near Hartree–Fock limit and density functional theory calculations

J. K. Deng, G. Q. Li, X. D. Wang, J. D. Huang, H. Deng, C. G. Ning, Y. Wang, and Y. Zheng

Citation: The Journal of Chemical Physics **117**, 4839 (2002); doi: 10.1063/1.1498816
View online: http://dx.doi.org/10.1063/1.1498816
View Table of Contents: http://scitation.aip.org/content/aip/journal/jcp/117/10?ver=pdfcov
Published by the AIP Publishing

Orbital electron densities of ethane: Comparison of electron momentum spectroscopy measurements with near Hartree–Fock limit and density functional theory calculations

J. K. Deng,[a] G. Q. Li, X. D. Wang, J. D. Huang, H. Deng, C. G. Ning, and Y. Wang
Department of Physics, Tsinghua University, Beijing 100084, People's Republic of China and Key Laboratory for Quantum Information and Measurements, MOE, People's Republic of China

Y. Zheng
Department of Chemistry, University of British Columbia, Vancouver, BC, V6T 1Z1, Canada

(Received 3 January 2002; accepted 14 June 2002)

Electron density distributions in momentum space of the valence orbitals of ethane (C_2H_6) are measured by electron momentum spectroscopy (EMS) in a noncoplanar symmetric geometry. The impact energy was 1200 eV plus binding energy and energy resolution of the EMS spectrometer was 0.95 eV. The measured experimental momentum distributions of the valence orbitals are compared with Hartree–Fock and density functional theory (DFT) calculations. The shapes of the experimental momentum distributions are generally quite well described by both the Hartree–Fock and DFT calculations when large and diffuse basis sets are used. A strong ''turn up'' of the experimental cross section is observed for the HOMO $1e_g$ orbital in the low momentum region, compared with the theoretical calculations. The pole strengths for the main ionization peaks in the inner-valence region are estimated. © *2002 American Institute of Physics.*
[DOI: 10.1063/1.1498816]

I. INTRODUCTION

Electron momentum spectroscopy (EMS) with symmetric noncoplanar geometry provides unique and detailed information on the electronic structures of atoms and molecules.[1–6] EMS can access the complete valance-shell binding energy range, though with lower resolution than that in most photoelectron spectroscopy (PES) studies, and the orbital electron density imaging information provided by EMS momentum profiles is unique. In particular, the electron momentum distribution information, obtained by the EMS technique, provides stringent tests for quantum chemical calculations at the Hartree–Fock level and also of correlated treatments such as density functional theory (DFT). Now a large body of EMS measurements is available for a wide variety of targets ranging from atoms to molecules such as amino acid glycine,[7] methylpropane,[8] pharmaceuticals amantadine,[9] and urotropine.[10] These results have convincingly shown that the interplay of EMS measurements and high level quantum mechanical calculations provides very detailed information on the binding energy, electronic structure, reactivity, and electron density distributions of electrons in atoms and molecules. In addition, it should be noted that the EMS technique is particularly sensitive to the low momentum part and thus the chemically important regions (i.e., outer spatial regions) of the outer valence (frontier) orbital electron density.

Ethane is formed by joining the two methyl groups and it has been an interesting target for studies of electronic structure because it is considered as a prototype of the single carbon–carbon bond, also as a prototype of tetrahedral (sp^3) hybridization in terms of the valence bond theory. Various PES studies were carried out for ethane and some controversy for the ground electronic state has been clarified.[11–15]

Two EMS studies have been carried out for ethane by Dey *et al.*[16] and Tian *et al.*,[17] respectively. Two impact energies, 400 and 1200 eV, were used by Dey *et al.* in their early experiments. The energy resolution of the EMS spectrometer was 1.5 eV at the 400 eV impact energy, and thus the binding energy spectra were not well resolved in the experiments. The experimental data were also modest because a single channel EMS spectrometer was used for the experiments. In the experiment of Tian *et al.*[17] the energy resolution of the EMS spectrometer was 1.67 eV and the three outer valence orbitals were not well resolved with such a poor energy resolution. The experimental data of the momentum distributions of the three outer valence orbitals, obtained by fitting Gaussians to the binding energy spectra, were scattered. Also, there were no high level calculations performed in the above two studies for ethane. Obviously, more accurate experimental data with a higher energy resolution and higher level SCF and DFT calculations are demanded.

The present work reports detailed experimental and theoretical investigations of the valence orbital electron densities of ethane. The impact energy is 1200 eV plus binding energy and the energy resolution is 0.95 eV. The complete valence shell binding energy spectra, from 10 to 34 eV, and the momentum profiles for the individual valence orbitals are obtained. Theoretical momentum distributions for all five valence orbitals are calculated by using the target Hartree–Fock approximation (THFA) and also with the target Kohn–Sham approximation (TKSA).[1–6] In the Hartree–Fock

[a]Electronic mail: djk-dmp@mail.tsinghua.edu.cn

calculations, three basis sets of STO-3G, 6-31G, and 6-311++G** are used. In the DFT calculations, hybrid functionals B3LYP and B3PW91 are used. The measured momentum profiles are compared with the HF and DFT calculations. In general, experiment and theory are in very good agreement. However, a significant difference between theory and experiment in the low momentum range is observed for the $1e_g$ orbital.

II. THEORETICAL BACKGROUND

In a binary $(e,2e)$ experiment, the scattered and the ionized electrons are detected at the same kinetic energies and the same polar angles in symmetric noncoplanar scattering geometry. Under conditions of high impact energy and high momentum transfer, the target electron essentially undergoes a clean ''knock-out'' collision and the plane wave impulse approximation (PWIA) provides a very good description of the collision. In the PWIA, the momentum p of the electron prior to knockout is related to the azimuthal angle by[1]

$$p=[(2p_1\cos\theta_1-p_0)^2+(2p_1\sin\theta_1\sin(\phi/2))^2]^{1/2}, \quad (1)$$

where $p_1=p_2=\sqrt{2E_1}$ is the magnitude of the momentum of each outgoing electron and $p_0=\sqrt{2E_0}$ is the momentum of the incident electron (both in atomic units). The EMS differential cross section in the PWIA for randomly oriented gas-phase molecules is given by[1]

$$\sigma_{\mathrm{EMS}}\propto S_f^2\int |\langle \mathbf{p}\Psi_f^{N-1}|\Psi_i^N\rangle|^2 d\Omega, \quad (2)$$

where $\mathbf{p}$ is the momentum of the target electron state prior to knockout, S_f^2 is pole strength defined in Ref. 18, and $|\Psi_f^{N-1}\rangle$ and $|\Psi_i^N\rangle$ are the total electronic wave functions for the final ion state and the target molecule ground (initial) state, respectively. The overlap of the ion and neutral wave functions in Eq. (2) is known as the Dyson orbital while the square of this quantity is $|\langle \mathbf{p}\Psi_f^{N-1}|\Psi_i^N\rangle|^2$ and is referred to as an ion-neutral overlap distribution (OVD) or Dyson orbital momentum density distribution. Thus, the EMS cross section is essentially proportional to the spherical average ($\int d\Omega$) of the square of the Dyson orbital in momentum space.

Therefore, Eq. (2) is greatly simplified by using the target Hartree–Fock approximation (THFA). Within the THFA, the many-body wave functions $|\Psi_f^{N-1}\rangle$ and $|\Psi_f^N\rangle$ are approximated as independent particle determinants of ground state target Hartree–Fock orbitals. The ion state is then in most cases dominated by a single hole in only one orbital and Eq. (2) can be simplified to

$$\sigma_{\mathrm{EMS}}\propto S_j^f\int |\psi_j(\mathbf{p})|^2\, d\Omega, \quad (3)$$

where $\psi_j(\mathbf{p})$ is the one-electron momentum space canonical Hartree–Fock orbital wave function for the jth electron, corresponding to the orbital from which the electron was ionized. S_j^f is the spectroscopic factor, the probability of the ionization event producing a one-hole configuration of the final ion state, estimates of S_j^f values can be obtained from a comparison of calculated and experimental cross sections. The integral in Eq. (3) is known as the spherically averaged one-electron momentum distribution (MD). Equation (2) has also been interpreted in the context of Kohn–Sham density functional theory.[19] The target Kohn–Sham approximation (TKSA) gives a result similar to Eq. (3) in which the canonical Hartree–Fock orbital is replaced by a momentum space Kohn–Sham orbital $\psi_j^{\mathrm{KS}}(\mathbf{p})$:

$$\sigma_{\mathrm{EMS}}\propto S_j^f\int |\psi_j^{\mathrm{KS}}(\mathbf{p})|^2\, d\Omega. \quad (4)$$

It should be noted that an accounting of electron correlation effects in the target ground state is included in the TKSA via the exchange correlation potential. A more detailed description of the TKSA–DFT method may be found elsewhere.[19] The TKSA approach has been compared with near Hartree–Fock limit and MRSD–CI overlap calculations and EMS measurements for the experimental momentum profiles of a large number of molecules (see, for example, Refs. 7–10).

In the present work, spherically averaged theoretical momentum profiles have been calculated for the valence orbitals of ethane using the PWIA. Details of the calculation methods are described below and the total number of contracted Gaussian-type orbital functions (CGTO) is also given for each calculation. The Hartree–Fock and DFT calculations were carried out using the GAUSSIAN 98 program. The Hartree–Fock calculations of the momentum profiles were performed by using Eq. (3) with the basis sets of STO-3G, 6-31G, and 6-311++G**. The B3LYP and B3PW91 functionals[20,21] are used for the two DFT calculations, respectively. Two basis sets of 6-31G and 6-311++G** are used for the B3LYP calculations while the truncated aug-cc-pVTZ basis set is used for the B3PW91 calculation.

(1) **STO-3G**: A calculation employing a minimal basis set (effectively single zeta). Each function is a contraction of three Gaussian functions and thus it consists of $C(6s,3p)/[2s,1p]$ and $H(3s)/[1s]$ contractions. Therefore, a total of 16 CGTO is employed for ethane. This basis set was designed by Pople and co-workers.[22]

(2) **6-31G**: The 6-31G basis of Pople and the co-workers[23] is a split-valence basis comprised of an inner valence shell of six *s*-type Gaussians and an outer valence shell that has been split into two parts represented by three and one primitives, respectively. Carbon atoms have a $(10s,4p)/[3s,2p]$ contraction and hydrogen atoms have a $(4s)/[2s]$ contraction. A total of 30 CGTO is used for ethane.

(3) **6-311++G****: The 6-311++G** is an augmented version by Pople *et al.* The outer valence shell is split into three parts and represented by three, one and one primitives. Very diffused *s* and *p* functions, and spherical *d* type polarization functions are added for carbon atoms, the full set of $6d$ Cartesian *d* functions have been used in the 6-311G** basis set. And a diffused *sp* shell and a *p*-type polarization functions are added for hydrogen atoms.[24–26] Thus a $(12s,6p,1d)$ contracts to $[5s,4p,1d]$ for C, and a $(6s,1p)$ to $[4s,1p]$ for H. The number of CGTO is 88 for ethane.

(4) **AUG-CC-pVTZ**: The basis set for these calculations was taken from the work of Dunning *et al.*[26–29] This basis set used in the present work is actually a truncated form

of Dunning's aug-cc-pVTZ basis set in which all *f*-, *g*-, and *h* functions have been removed. The full set of 6*d* Cartesian *d* functions have been used in the 6-311G** basis set. Thus, it consists of C(33*s*,13*p*,5*d*)/[7*s*,6*p*,5*d*] and H(13*s*,5*p*)/[6*s*,5*p*] contractions per atom. The *d* functions are Cartesian. Thus, a total of 236 CGTO is used for ethane.

III. EXPERIMENTAL METHODS

The details and operation of the symmetric noncoplanar, energy dispersive, multichannel EMS spectrometer used in this work have been described in detail[30] and thus only a brief outline will be given here. The gas-phase target molecules ($\sim 10^{-5}$ torr) are ionized by impact with a high energy electron beam ($E_0 = 1200$ eV plus binding energy). Two outgoing electrons (scattered and ionized) are electron optically retarded, selected energetically by electrostatic analyzers and detected in coincidence by microchannel plate position sensitive detectors mounted on two independent horizontal concentric turntables. In the symmetric noncoplanar scattering geometry, the two outgoing electrons are selected to have equal polar angles ($\theta_1 = \theta_2 = 45°$) relative to the forward scattered electron beam. One analyzer turntable is kept in a fixed position while the other is rotated by a computer controlled stepping motor. Each electron energy analyzer accepts a range of kinetic energies from 596 to 604 eV simultaneously, but only those coincident electron pairs with summed energies in the range of 1200 ± 3.5 eV are recorded.[30]

In present EMS measurements the individual orbitals are selected by the choice of the binding (or ionization) energy. In order to obtain the experimental momentum profiles corresponding to the main peaks in the outer and inner valence regions with the multichannel energy dispersive spectrometer, wide range binding energy spectra (BES) are collected at a series of azimuthal (out of plane) angles ϕ over the range of 0° to ±30° in a series of sequential repetitive scans.

Momentum distributions as a function of angle ϕ are obtained by deconvolution of these binding energy spectra using Gaussian functions located at each ionization energy in the BES. The widths and relative position of the Gaussian functions can be determined from a consideration of published high resolution PES vibronic manifolds and the EMS instrumental energy resolution function (0.95 eV FWHM). For each ionization process, the area of the fitted peak (or the integral of the spectral region, where appropriate) is plotted as a function of momentum calculated from ϕ using Eq. (1). A given set of areas as a function of momentum for a specific binding energy is referred to as an experimental momentum profile (XMP). To compare the XMPs with the relative cross-sections calculated as a function of momentum using expressions (2) and (3) above, the effects of the finite spectrometer acceptance angles in both θ and ϕ ($\Delta\theta = \pm 0.6°$ and $\Delta\phi = \pm 1.2°$) were included in the calculations. This is achieved in the present work by using the Gaussian-weighted planar grid method of Duffy *et al.*[31] After momentum resolution folding, the calculation [Eqs. (2), (3) or (4)] is referred to as a theoretical momentum profile (TMP). The molecular geometry used in all calculations for ethane was from Snyder and Basch.[32]

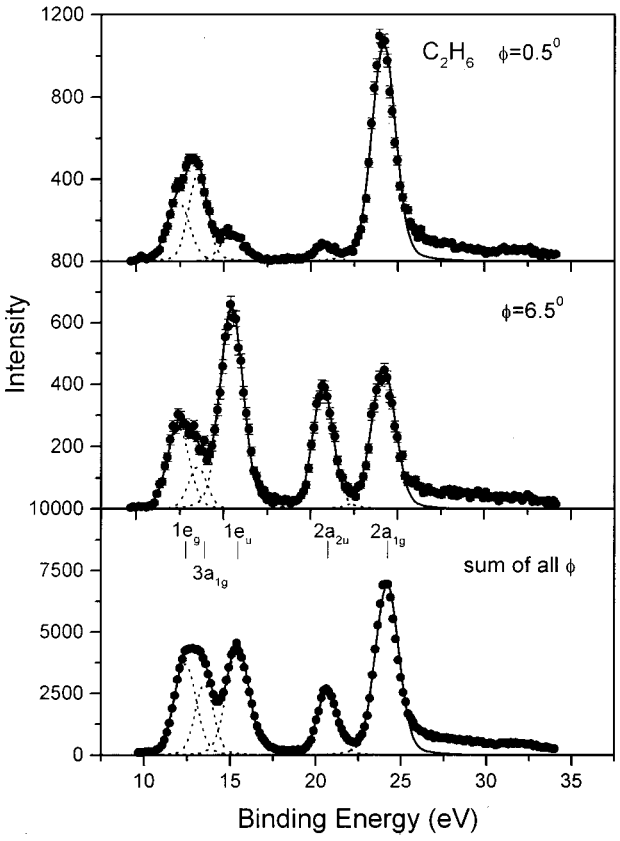

FIG. 1. EMS binding energy spectra of ethane from 10 to 34 eV at (a) $\phi = 0.5°$, (b) $\phi = 6.5°$, and (c) summed over all 17 ϕ angles, obtained at an impact energy of (1200 eV+binding energy). The dashed lines represent Gaussian fits to the peaks and the solid curve is the summed fit.

All multichannel measurements in the present work were obtained using the "binning" mode.[33] The ethane sample was reagent grade (>99.0% purity) and was used without further purification other than freeze–thaw cycles to remove dissolved air. No impurities were observed in any of the binding energy spectra.

IV. RESULTS AND DISCUSSION

Ethane belongs to the D_{3d} point group and the Hartree–Fock (independent particle) ground state valence electron configuration can be written as

$$\text{Core}(2a_{1g})^2(2a_{2u})^2(1e_u)^4(3a_{1g})^2(1e_g)^4.$$

There are two degenerate and one nondegenerate outer valence molecular orbitals, and two nondegenerate orbitals in the inner valence. The order and assignment of the valence orbitals are from the He I PES study reported by Kimura *et al.*[12]

Figure 1 shows the binding energy spectra from 10 to 34 eV, for the two individual relative azimuthal angles of $\phi = 0.5°$ and $\phi = 6.5°$, respectively, and also for sum of all azimuthal angles (impact energy of 1200 eV plus binding energy) on a common intensity scale. The energy resolution of the EMS spectrometer was 0.95 eV FWHM. The energy scale in Fig. 1 was calibrated with respect to the $(1e_g)^{-1}$ vertical ionization potential as measured by high resolution

TABLE I. Ionization energies (eV) for ethane.

Orbital	Experiment				Theoretical orbital energies of HF/6-311++G** [a]
	EMS[a]	PES[b]	EMS[c]	EMS[d]	
$1e_g$	12.40	11.99 (12.70)	12.25	12.2	13.28
$3a_{1g}$	13.5	13.5	13.35	13.5	13.86
$1e_u$	15.45	15.15 (15.90)	15.45	15.5	16.27
$2a_{2u}$	20.7	20.1	21.0	20.3	22.98
$2a_{1g}$	24.2		24.5	24.0	27.72

[a]This work.
[b]From Ref. 12.
[c]From Ref. 16.
[d]From Ref. 17.

photoelectron spectroscopy.[12] Five Gaussian functionals have been fitted to the binding energy spectra in Fig. 1. The position and width of each Gaussian peak were obtained by using vertical ionization potentials and Franck–Condon widths (folded with the EMS instrumental energy width of 0.95 eV FWHM) estimated from photoelectron spectroscopy measurements.[12] The relative energy spacings of the Gaussian peaks were estimated from the vertical ionization potentials, with small adjustments to compensate for the asymmetries in the shapes of the Franck–Condon envelopes. The measured ionization potentials of this work and early published data[12,16,17] and the Hartree–Fock values are compared in Table I.

The removal of a $1e_g$ electron leading to the ground state of the ion produces the band (Fig. 1) at 12.4 eV which is more intense at $\phi=6.5°$ than at $\phi=0.5°$ in the EMS binding energy spectra. The second orbital $3a_{1g}$ at 13.5 eV results in an ''*s*-type'' band which is of much higher intensity at $\phi=0.5°$ than that at $\phi=6.5°$. The band located at 15.45 eV corresponds to the ionization of the $1e_u$ orbital. Obviously this orbital has a ''*p*-type'' character from the two angle binding energy spectra in Fig. 1. The ionization peaks for the two inner valence orbitals, $2a_{2u}$ and $2a_{1g}$, are at 20.7 and 24.2 eV, respectively. From the experimental EMS binding energy spectra at $\phi=0.5°$ and $\phi=6.5°$ there is some ionization intensity extending out from 25 eV to the limit of the data at 34 eV. The higher intensity at $\phi=0.5°$ than that at $\phi=6.5°$ implies that the *s*-type $(2a_{1g})^{-1}$ ionization process is dominant in the energy region.

Experimental and theoretical spherically averaged momentum profiles have been obtained for the valence orbitals of ethane. Experimental momentum profiles are extracted from the sequentially obtained, angular-correlated, multichannel (binning mode) binding energy spectra, and therefore the relative normalizations for the different transitions are maintained. The Gaussian fitting procedure, described above for the binding energy spectra, is used to determine the relative intensities of the various orbital ionizations at each azimuthal angle ϕ. The experimental momentum profile for a particular orbital is obtained by plotting the area under the corresponding fitted peak for each electronic state of the ion as a function of p. With this procedure all momentum profiles are automatically placed on a common relative intensity scale. Various theoretical momentum profiles (TMPs) of the valence orbitals are obtained as described in Sec. II.

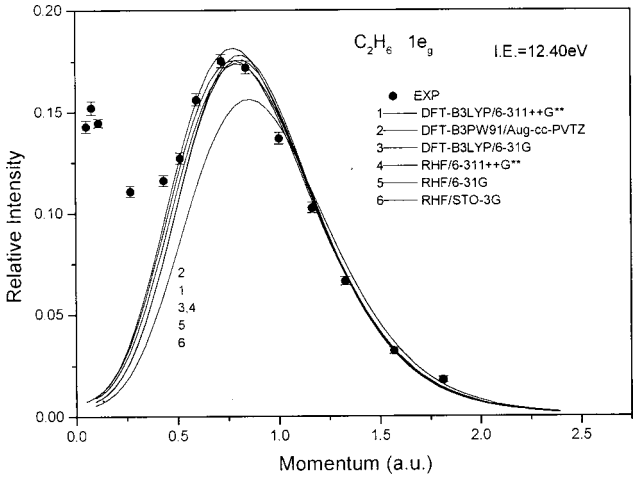

FIG. 2. Measured and calculated spherically averaged momentum profiles for the $1e_g$ orbital of ethane. The solid circles represent the experimental energy dispersive multichannel measurements. All calculations have been spherically averaged and folded with the experimental momentum resolution.

The finite experimental momentum resolution ($\Delta p \sim 0.1$ a.u.) is also folded into the TMPs by using the GW–PG method.[31] The experimental and the theoretical momentum profiles have been placed on a common intensity scale by normalizing the experimental data for the HOMO $(1e_g)$ orbital to the B3PW91/aug-cc-pVTZ DFT TMP in Fig. 2. The same normalization factor obtained in this procedure is then used for each individual orbital for all experimental and theoretical comparisons.

The theoretical and experimental momentum profiles of all the valence orbitals of ethane are presented in Figs. 2–8 using the above normalization. In the following discussion the comparisons between the theoretical calculations and the experimental data are provided for the outer valence orbitals and inner valence orbitals in turn.

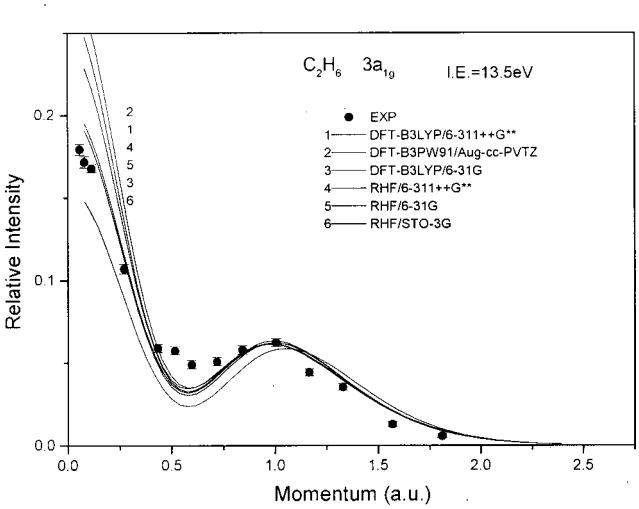

FIG. 3. Measured and calculated spherically averaged momentum profiles for the $3a_{1g}$ orbital of ethane. The solid circles represent the experimental energy dispersive multichannel measurements. All calculations have been spherically averaged and folded with the experimental momentum resolution.

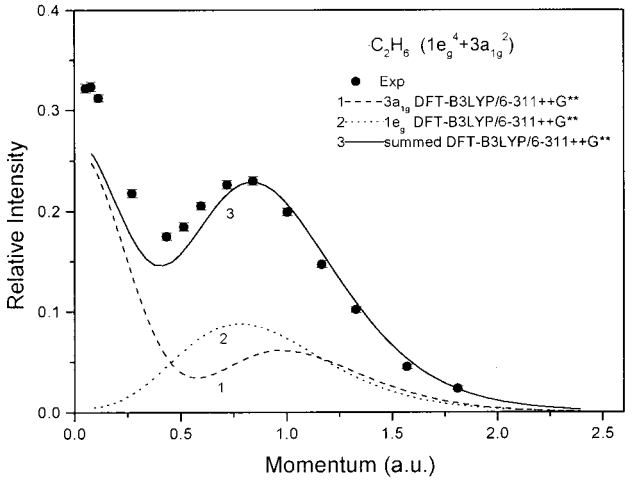

FIG. 4. Measured and calculated spherically averaged momentum profiles for the sum of the $(1e_g+3a_{1g})$ orbitals of ethane. The solid circles represent the experimental energy dispersive multichannel measurements. All calculations have been spherically averaged and folded with the experimental momentum resolution.

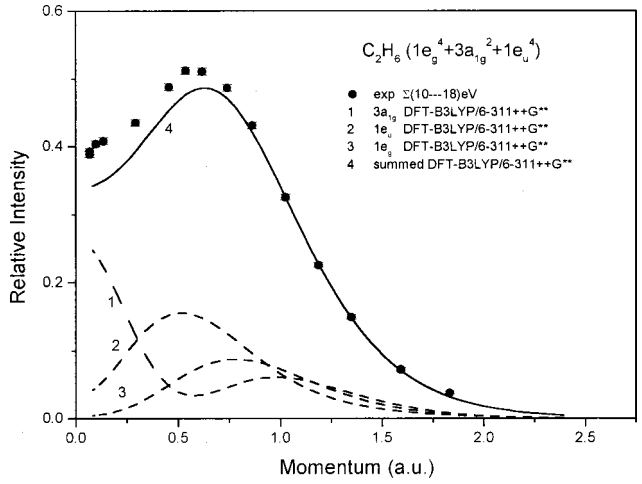

FIG. 6. Measured and calculated spherically averaged momentum profiles for the sum of the $(1e_g+3a_{1g}+1e_u)$ orbitals of ethane. The solid circles represent the experimental energy dispersive multichannel measurements. All calculations have been spherically averaged and folded with the experimental momentum resolution.

The HOMO of ethane is associated with the $1e_g$ electrons which, in simple valence bond terms, would be considered to be the carbon ''lone pair'' nonbonding electrons. The experimental and the theoretical momentum profiles for the $1e_g$ orbital of ethane are shown in Fig. 2. The experimental and the theoretical momentum profiles show the expected *p*-type distribution (the experimental $p_{\max}\sim 0.8$ a.u.). As can be seen, in the momentum region from 0.5 to 2.0 a.u., the better quality of wave function is, the closer agreement with the experimental data gets. The DFT momentum profiles (curves 1 and 2 in Fig. 2) are almost the same in both intensity and shape, and model the XMP very well.

However, there is a significant discrepancy between experiment and theory in the low momentum region below 0.5 a.u. The experimental data shows a strong ''*s*-type'' turn up and all calculations underestimate the experimental intensity in the momentum region. The higher experimental intensity in the region is possibly due to ''contamination'' from the neighboring relatively intense ''*s*-type'' second outermost $(3a_{1g})$ orbital caused by an error in the curve fitting and deconvolution procedures.

This explanation seems to be supported from comparison of the XMP of the $3a_{1g}$ orbital with the calculations in Fig. 3 where, except for the STO-3G calculation, all other calculations overestimate the experimental intensity in the momentum region below 0.4 a.u. and reasonably reproduce the experimental data above 0.5 a.u. In order to further investigate the explanation, the summed experimental data of the $1e_g$ and $3a_{1g}$ orbitals is compared with the summed DFT–B3LYP/6-311++G** TMP in Fig. 4. Again, the summed TMP gives a very reasonable description for the

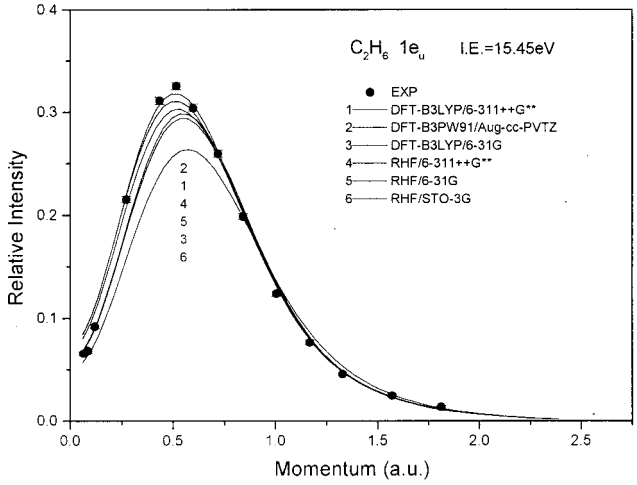

FIG. 5. Measured and calculated spherically averaged momentum profiles for the $1e_u$ orbital of ethane. The solid circles represent the experimental energy dispersive multichannel measurements. All calculations have been spherically averaged and folded with the experimental momentum resolution.

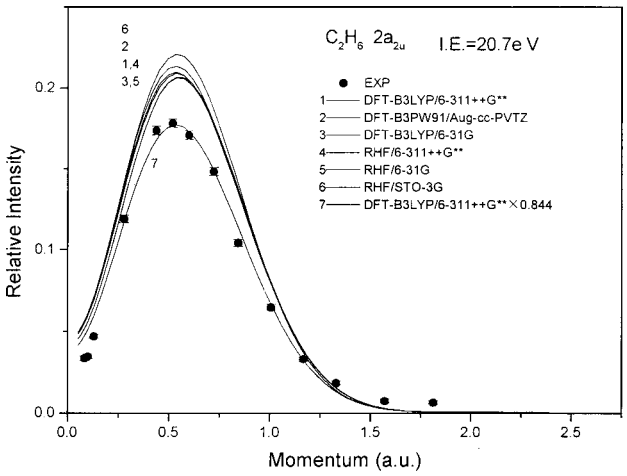

FIG. 7. Measured and calculated spherically averaged momentum profiles for the $2a_{2u}$ orbital of ethane. The solid circles represent the experimental energy dispersive multichannel measurements. All calculations have been spherically averaged and folded with the experimental momentum resolution.

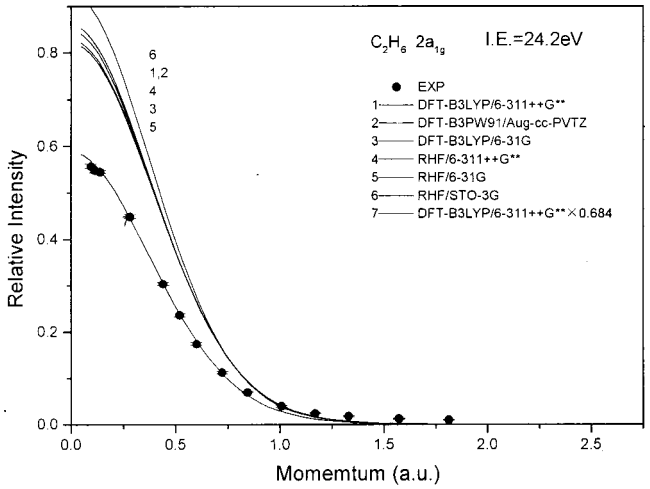

FIG. 8. Measured and calculated spherically averaged momentum profiles for the $2a_{1g}$ orbital of ethane. The solid circles represent the experimental energy dispersive multichannel measurements. All calculations have been spherically averaged and folded with the experimental momentum resolution.

summed XMP above 0.7 a.u., and significantly underestimates the experimental data below 0.6 a.u. This indicates that the discrepancy between experimental data and theoretical calculation below 0.5 a.u. for the $1e_g$ orbital is not mainly due to a possible error in the curve fitting and deconvolution procedures.

A consideration of the relative phase in the position space wave function topograph for the $1e_g$ orbital indicates this orbital has strong π^*-like character. It has been found[34,35] that such orbitals usually produce a ''turn up'' of the cross section in the low momentum range, and this behavior is similar to the low-*p* effect observed in atomic *d*-orbital XMPs. This situation is also probably the case for the $1e_g$ orbital of ethane. Theoretical studies of atomic targets[36] have convincingly shown that such effects in *d* orbitals are due to breakdown of the plane wave impulse approximation (PWIA) caused by significant low momentum components near the nucleus which can occur in orbitals of grads symmetry for $l \geqslant 2$. Distorted wave calculations[36] have predicted that such effects will diminish with increase of impact energy above the commonly used value of 1200 eV and that they will become negligible above a few keV. Unfortunately, at present, DWIA calculations are possible only for atoms but not for molecules due to the multicenter nature of the latter.

Experimental and theoretical momentum profiles for the $1e_u$ orbital are shown in Fig. 5. Both the experimental and theoretical momentum profiles show ''*p*-type'' momentum distributions for the orbital. The agreement between the two DFT calculations (curves 1 and 2 in Fig. 5) and experimental data is quite good. Other Hartree–Fock calculations (curves 3, 4, and 5 in Fig. 5), except for the HF/STO-3G calculation (curve 6), reproduce the experimental data very well. In order to further confirm the conclusion that the ''turn up'' of the $1e_g$ orbital in the low momentum region is not mainly due to possible errors in the curve fitting and deconvolution procedures, the summed experimental data of the $1e_g$, $3a_{1g}$, and $1e_u$ orbitals is compared with the summed DFT-B3LYP/6-311++G** TMP in Fig. 6. Again, the summed TMP gives a very reasonable description for the summed XMP above 0.7 a.u. and significantly underestimates the experimental data below 0.6 a.u. This shows that the discrepancy between experiment and theory below 0.5 a.u. for the $1e_g$ orbital is not mainly due to a possible error in the curve fitting and deconvolution procedures and there are other sources to cause the significant discrepancy in the low momentum region. A possible source could be that the distorted wave effect causes the significant discrepancy in the momentum region.

The experimental and theoretical momentum profiles for the $2a_{2u}$ and $2a_{1g}$ orbitals of ethane are shown in Figs. 7 and 8, respectively. It should be noted that the energy positions and widths for the $2a_{2u}$ and $2a_{1g}$ orbitals, used in the deconvolution procedure, are not based on published photoelectron spectra, but rather on an estimate from the present molecular orbital calculations and the fitting quality of the individual binding energy spectra (Fig. 1) collected at different ϕ angles. A comparison of the intensities of the experimental and theoretical momentum profiles in Figs. 7 and 8 shows that the $(2a_{2u})^{-1}$ and $(2a_{1g})^{-1}$ ionization processes have been split into higher energy satellite ''poles'' due to strong electron correlation processes. The ''*p*-type'' character is consistent with the assignment of the peak at 20.7 eV in the EMS binding energy spectrum (see Fig. 1). The comparison between experiment and theory for the $2a_{2u}$ orbital is shown in Fig. 7 in which the theoretical calculations generally describe the shape of the experimental momentum profile. The curve 7, obtained by multiplying curve 1 by a factor of 0.844, is in very good agreement in shape with the experimental data. This indicates that the remaining 0.156 pole strength has been split into higher energies. The experimental and theoretical momentum profiles of the orbital $2a_{1g}$ show strong ''*s*-type'' distributions in Fig. 8. The peak at ~24.2 eV at $\phi=0°$ EMS binding energy spectrum (Fig. 1) could be mainly attributed to ionization from the $2a_{1g}$ orbital (although the presence of other satellite ionization processes within this peak area cannot be entirely discounted). The calculated momentum profiles from Hartree–Fock and density function theory give a similar shape with the XMP. Similarly, curve 7 (multiplying curve 1 by 0.684) in Fig. 8 is in good agreement with the experiment in shape. The presence of a high energy ''tail'' out to the limit of the data at 34 eV observed in the EMS binding energy spectra (see Fig. 1) also supports the view that higher energy poles exist.

V. SUMMARY

In summary, the detailed experimental and theoretical investigations of the valence orbital electron densities of ethane by electron momentum spectroscopy are reported. The experimental momentum distributions are compared with the associated calculations. The binding energies are in excellent agreement with previously published PES data. The experimental momentum profiles are described by Hartree–Fock 6-311++G** calculations. The density functional theory (DFT) calculations using B3LYP and B3PW91 functions provide the best description to the experiments. A

strong discrepancy between theoretical calculations and experimental data is observed for the momentum distributions of the $1e_g$ orbital in the low momentum region due to possible distorted wave effects.

ACKNOWLEDGMENTS

This work is supported by the National Natural Science Foundation of China under Grant Nos. 19854002 and 19774037 and the Research Fund for the Doctoral Program of Higher Education under Grant No. 1999000327. The authors would also like to acknowledge help and useful discussion from Professor C. E. Brion and Professor Zhu Qihe.

[1] I. E. McCarthy and E. Weigold, Rep. Prog. Phys. **91**, 789 (1991).
[2] C. E. Brion, Int. J. Quantum Chem. **29**, 1397 (1986).
[3] C. E. Brion, in *The Physics of Electronic and Atomic Collisions*, edited by T. Anderson *et al.* (American Institute of Physics, New York, 1993), p. 350.
[4] C. E. Brion, G. Cooper, Y. Zheng, I. V. Litvinyuk, and I. E. McCarthy, Chem. Phys. **270**, 13 (2001).
[5] K. T. Leung, in *Theoretical Models of Chemical Bonding*, edited by Z. B. Maksic (Springer-Verlag, Berlin, 1991), p. 339.
[6] A. O. Bawagan *et al.*, Chem. Phys. **113**, 19 (1987).
[7] Y. Zheng, J. J. Neville, and C. E. Brion, Science **270**, 786 (1995).
[8] J. K. Deng *et al.*, J. Chem. Phys. **114**, 882 (2001).
[9] I. V. Litvinyuk, Y. Zheng, and C. E. Brion, Chem. Phys. **261**, 289 (2000).
[10] I. V. Litvinyuk *et al.*, Chem. Phys. **263**, 195 (2001).
[11] A. D. Baker *et al.*, Int. J. Mass Spectrom. Ion Phys. **1**, 285 (1968).
[12] K. Kimura, S. Katsumata, Y. Achiba, T. Yamazaki, and S. Iwata, *Handbook of HeI Photoelectron Spectra of Fundamental Organic Molecules* (Japan Scientific Society, Tokyo, 1981).
[13] J. W. Rabalais and A. Katrib, Mol. Phys. **27**, 923 (1974).
[14] K. Hamrin *et al.*, Chem. Phys. Lett. **1**, 613 (1968).
[15] B. Narayan, Mol. Phys. **27**, 923 (1974).
[16] S. Dey *et al.*, J. Electron Spectrosc. Relat. Phenom. **9**, 397 (1976).
[17] S. X. Tian *et al.*, J. Phys. B **31**, 2055 (1998).
[18] Y. Zheng *et al.*, Chem. Phys. **212**, 269 (1996).
[19] P. Duffy *et al.*, Phys. Rev. A **50**, 4704 (1994), and references therein.
[20] J. P. Perdew and Y. Wang, Phys. Rev. B **33**, 8800 (1986).
[21] A. D. Becke, Phys. Rev. A **38**, 3098 (1988).
[22] W. J. Hehre, R. F. Stewart, and J. A. Pople, J. Chem. Phys. **51**, 2657 (1969).
[23] R. Krishnan, M. J. Frisch, and J. A. Pople, J. Chem. Phys. **72**, 4244 (1980).
[24] T. Clark *et al.*, J. Comput. Chem. **4**, 294 (1983).
[25] M. J. Frisch, J. A. Pople, and J. S. Binkley, J. Chem. Phys. **80**, 3265 (1984).
[26] T. H. Dunning, Jr., J. Chem. Phys. **90**, 1007 (1989).
[27] R. A. Kendall, T. H. Dunning, Jr., and R. J. Harrison, J. Chem. Phys. **96**, 6796 (1992).
[28] D. E. Woon and T. H. Dunning, Jr., J. Chem. Phys. **98**, 1358 (1993).
[29] D. E. Woon and T. H. Dunning, Jr., J. Chem. Phys. **99**, 1914 (1993).
[30] Y. Zheng *et al.*, J. Chem. Phys. **111**, 9526 (1999).
[31] P. Duffy *et al.*, Chem. Phys. **159**, 347 (1992).
[32] L. C. Snyder and H. Basch, *Molecular Wave Functions and Properties* (Wiley, New York, 1972).
[33] Y. Zheng *et al.*, Chem. Phys. **188**, 109 (1994).
[34] C. E. Brion *et al.*, J. Phys. B **31**, L223 (1998).
[35] J. Rolke *et al.*, Chem. Phys. **244**, 1 (1999).
[36] M. J. Brunger *et al.*, J. Phys. B **27**, L597 (1994).